



Article

Unveiling the Subsurface of Late Amazonian Lava Flows at Echus Chasma, on Mars

Federico Mansilla ^{1,*} , María-Paz Zorzano ¹ , Iraklis Giannakis ² and Javier Ruiz ³¹ Centro de Astrobiología (CSIC-INTA), Torrejón de Ardoz, 28850 Madrid, Spain² Department of Geology and Geophysics, University of Aberdeen, Meston Building, Kings College, Aberdeen AB24 3EU, UK³ Departamento de Geodinámica, Estratigrafía y Paleontología, Universidad Complutense de Madrid, 28040 Madrid, Spain* Correspondence: fmansilla@cab.inta-csic.es

Abstract: The Echus-Kasei region on Mars has been exposed to different episodic volcanic, fluvial, and glacial events in Amazonian time. The goal of the present work is to demonstrate the usefulness of radar instruments to find preserved late Amazonian subsurface structures that may have been encapsulated underneath recent lava flows on Mars. We have analysed 27 radar observations of the SHallow RADar (SHARAD) instrument on board the Mars Reconnaissance Orbiter (MRO), over the region of Echus Chasma. We discovered the presence of subsurface reflectors in five consecutive SHARAD radargrams at a depth from 35 to 79 m beneath the structure of a lava fan that formed about 59 ± 4 Ma ago. Some vents are preserved above the surface of this lava flow, which stands at a height of 80 m above the surrounding surface. A few kilometres to the north, we find other subsurface reflectors at a depth of about 30 m and a long pit chain formed by the collapse of a lava tube. These kinds of subsurface late Amazonian structures are of interest for astrobiology because they date from the last period when the planet still experienced intense volcanic activity over regions that were previously extensively covered by water.

Keywords: radar; Mars; lava; Amazonian

Citation: Mansilla, F.; Zorzano, M.-P.; Giannakis, I.; Ruiz, J. Unveiling the Subsurface of Late Amazonian Lava Flows at Echus Chasma, on Mars. *Remote Sens.* **2023**, *15*, 1357. <https://doi.org/10.3390/rs15051357>

Academic Editor: Christian Wöhler

Received: 27 January 2023

Revised: 20 February 2023

Accepted: 24 February 2023

Published: 28 February 2023



Copyright: © 2023 by the authors. Licensee MDPI, Basel, Switzerland. This article is an open access article distributed under the terms and conditions of the Creative Commons Attribution (CC BY) license (<https://creativecommons.org/licenses/by/4.0/>).

1. Introduction

During the most recent history of Mars (namely, the Amazonian epoch), there had been some episodic periods where water, ice, and lava flows may have coexisted or partially overlapped on its surface, rendering the surface of Mars active and potentially habitable [1–3]. In particular, previous research of Echus Chasma and the Kasei Valles has shown that this region was affected by at least four episodes of widespread volcanic activity and four periods of episodic fluvio-glacial activity from the Hesperian to the Amazonian Epochs on Mars (from 3.6 Ga to present) [4,5]. The last of the four major volcanic episodes occurred around 90 Ma between the last two episodes of fluvio-glacial activity [4]. This work shows evidence suggesting that glaciers and near-surface ice may have persisted through Amazonian times in local areas over the entire length of the Kasei Valles, and that it was covered by what is now seen as a platy-flow surface material interpreted to be 2100 km runout flood lavas sourced from the Echus Chasma.

More recent research of the Kasei Valles region around 27°N indicates that 1400–3500 km³ of ice were present at the time the lava was emplaced, about 1.3 Ga [3]. Viscous flow features (interpreted as ice-rich deposits buried beneath the sediment mantle [3]) can be located there today, including lobate debris aprons [6]. This region contains geomorphological evidence of lava-ice interactions in the form of depressions surrounding isolated mesas or situated parallel to scarps [7]. These depressions are formed when ice and lava interact, and mark the extent of ice-rich glaciers at the time the lava flow was formed. The dating of these structures suggests that ice survived for up to ~1 billion years following lava emplacement

before its final demise [3]. Its long-term survival was presumably aided by supraglacial debris layers like those on present-day glacier landforms on Mars. These regions represent some of the oldest large glacial ice masses on Mars.

The youngest crater retention ages on the floor of Echus Chasma suggest an age between 54 and 98 Ma [4]. It is noticeable that the most recent activity at Arsia Mons (the southernmost of three volcanoes on Tharsis) peaked at 150 Ma and ceased by 10–90 Ma [8]. This dating was done by studying the fresh lava flows of 29 volcanic vents within the Arsia Mons caldera. Volcanic vents in this study area are located on topographic highs and show lavas emanating from them. Thicknesses of lava flows on Arsia Mons' flanks have been estimated to be from about 10 to 80 m [9].

Other studies [10–12] have discussed the age, structures, and dielectric properties of lava flows on the western flanks of Ascraeus Mons (the northernmost of three Tharsis Montes volcanoes). These studies have described the existence of subsurface reflectors underneath the western flank.

In the present work, we focus on the eastern flank of Ascraeus Mons, in particular the Echus-Kasei system (Figure 1). Our main goal is to demonstrate the usefulness of orbital radar sounders to find reflectors that may inform us on the presence of preserved subsurface layers underneath the most recent lava flows. This would be extremely interesting for astrobiology because the existence of reflectors indicates changes in the subsurface properties, which may be due to changes in porosity or composition [13]. Subsurface encapsulated layers, formed over regions that were previously covered by water, may have been habitable and protected from desiccation and cosmic radiation until now. The second objective of this work is to find caves [14] or lava tubes associated with these lava flows that may be used as settlements for the future human exploration of Mars to avoid the extreme levels of cosmic radiation at surface level [15–17].

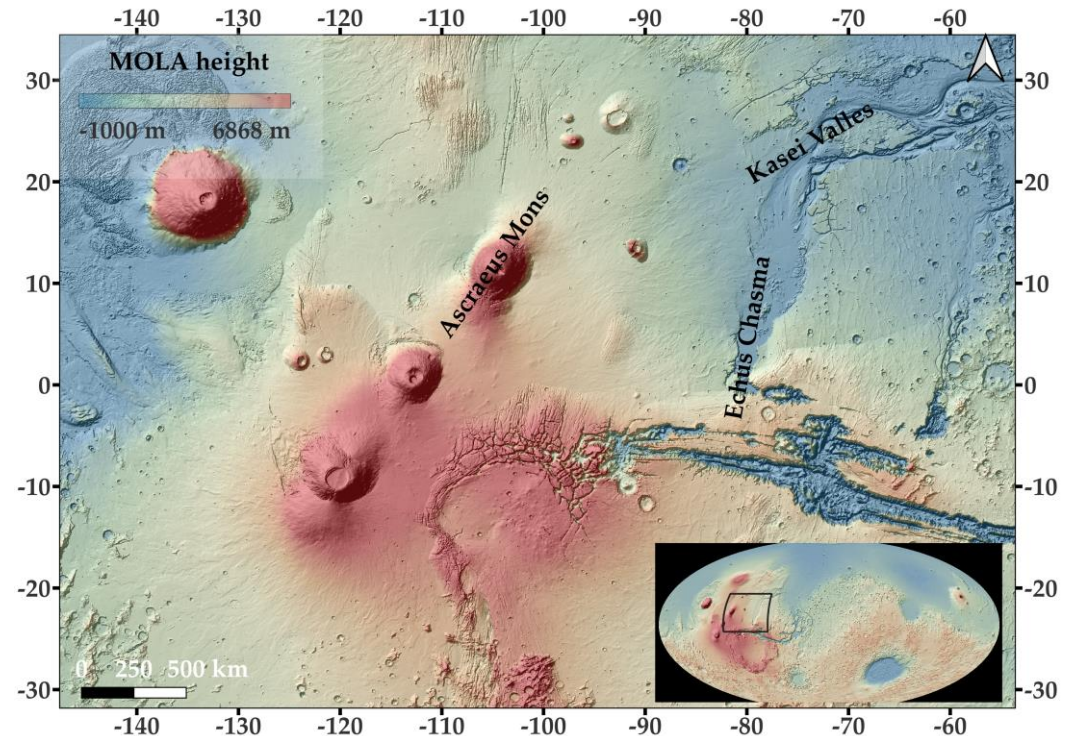


Figure 1. MOLA-derived situation map of the area of study, where the three main features of interest are located: Ascraeus Mons as the source area, Echus Chasma, where the dated lava fan is located, and Kasei Valles.

In the long term, this research has two purposes: (1) to demonstrate the usefulness of combining radar data with other instruments and (2) to establish a methodology that can be extended to analyze the entire surface of Mars.

The material and methods used in this work are presented in Section 2. The specific objectives of this work are covered in Section 3.1, where we describe the discovery of new lava flows in the Echus-Kasei system, collect the radargrams with confirmed reflectors and calculate the thickness of these lava flows; in Section 3.2 we date the lava flow structure using the crater counting method; in Section 3.3 we discuss the potential depth of the subsurface reflectors; and in Section 3.4 we investigate the possible presence further north of other lava-related features, well within the Echus-Kasei system. Finally, Section 4 presents a discussion of the results and analysis presented and Section 5 makes a summary of the findings of this work.

2. Materials and Methods

We first perform a visual survey of the region of interest in order to find surface features that may be indicative of lava flows. We use four global datasets to achieve this: (1) Mars Orbital Laser Altimeter (MOLA) topography [18], (2) High-Resolution Stereo Camera (HRSC) [19] image mosaics and topography derived, (3) Context Camera (CTX) mosaic developed by the Bruce Murray Laboratory for Planetary Visualization [20], and (4) Thermal Emission Imaging System (THEMIS), an infrared, daytime mosaic [21]. We analyse the data with QGIS [22] and JMARS [23]. QGIS is a geospatial information system developed by the QGIS Development Team. JMARS is a geospatial information system developed by the Mars Space Flight Facility of Arizona State University. We then investigate the radargrams provided by the SHallow RADar (SHARAD) instrument on board the Mars Reconnaissance Orbiter (MRO).

MOLA is a payload onboard the Mars Global Surveyor (MGS) spacecraft, launched in 1996, and it was in operation, collecting altimetry data, until June 30, 2001. It measured the travel times of a laser ray emitted from the instrument to the surface of Mars, allowing the construction of the Digital Elevation Models (DEMs) of the surface of Mars. The *Mars MGS MOLA DEM 463 m v2* has a spatial resolution of 463 m/px.

The High-Resolution Stereo Camera (HRSC) experiment carried on the Mars Express mission, launched on 2 June 2003, is a stereo camera experiment that allows for the creation of photogrammetrically controlled digital elevation models of the surface of Mars with spatial resolutions ranging between 10 and 30 m. In this work, HRSC was only used for the preliminary surveys as there are no Digital Elevation Models (DEMs) available for the region of interest.

CTX is the Context Camera, onboard the Mars Reconnaissance Orbiter (MRO). It was designed to complement the HiRISE (High Resolution Imaging Science Experiment), another camera experiment onboard MRO with stereo capabilities and a very high resolution (up to 30 cm/px) for the localisation of features in a wide field. The mosaic used was developed by the Murray Lab (the Bruce Murray Laboratory for Planetary Visualisation) at the California Institute of Technology and consists of a seam-corrected and seam-mapped mosaic of Mars rendered at 5 m/px. This product has been used to implement the largest-scale surveys.

THEMIS is an instrument that combines two independent multispectral imaging systems, one with 5 bands in the visible range and another with 10 bands for the infrared imaging system. It was carried by the Mars Odyssey mission, launched on 7 April 2001, and it is still operational today. It is useful for mineral identification using visible and infrared information. We used the derived product, *Thermal Emission Imaging System (THEMIS), a daytime infrared (IR) 100 m/pixel mosaic (version 12)*, released in the summer of 2014 by Arizona State University, to identify features at a small scale.

The Shallow Radar experiment aboard the Mars Reconnaissance Orbiter mission is known as SHARAD. This instrument had been designed to look for frozen or liquid water under the first kilometre of the Martian surface. It uses a 10 m antenna that transmits

“chirps” of 85 microseconds at frequencies between 15 and 25 megahertz [24]. With this technology, it is capable of detecting features at a vertical resolution of 10 m and a horizontal resolution of between 0.3 and 3 km.

Ground-penetrating radar systems have been extensively used to investigate the subsurface of Mars, find water reservoirs, as well as identify possible reflectors that inform on the structure of the uppermost layers of the planet. The two radar systems that have been investigating Mars are MARSIS [25], onboard Mars Express, and SHARAD [24] onboard the Mars Reconnaissance Orbiter. SHARAD has been in operation since November 2006. These instruments transmit low-frequency radio waves that penetrate the subsurface and receive the reflected signal. The difference in the reflected power is due to the different dielectric properties of the materials traversed by the signal. This technique is very useful to remotely investigate the geometry and nature of discontinuities. Cluttergrams are needed to discriminate the echoes from the surface topography from those from true reflectors. Once we have identified potential subsurface reflectors in the radargrams of the region of interest, we make the corresponding cluttergrams of the radargrams for comparison, in order to avoid false positives [26,27]. We first do our own survey, applying the cluttergram method described by Choudahary et al. [27,28]. In order to base the analysis on an open access cluttergram, we use CO SHARPS, the cluttergram-generating code applied to SHARAD data by the instrument team [29]. Both radargrams and cluttergrams are archived in the Planetary Data System node for SHARAD [30,31].

The age of the lava flow is calculated using the crater counting method [32–35]. To apply it, we digitize the craters within the region of interest, paying attention to their shape. We export the shapefiles with the CSFD tool, which is designed to make crater size-frequency distribution measurements using polygonal-shape files in a format useful for working in Craterstats [36]. This workflow permits the use of any GIS tool to make the crater survey. We work with QGIS because it is open-source software widely used in planetary sciences, and its digitizing tools are very useful and user-friendly. Once we have the crater survey, we make the statistical analysis using Craterstats 2.0 and by applying the chronology system proposed by *Hartmann and Daubar, 2017* [37]. The crater counting results are compared with the Martian epochs proposed by *Michael in 2013* [35]. With these constraints, we plot the results of the cumulative crater count using a diameter range between 100 and 1000 m and a pseudo-logarithmic scale.

Finally, the depth of reflectors is estimated by converting the time delay Δt (in seconds) to the height Δh (in meters) using the following equation $\Delta h = c\Delta t / \sqrt{\epsilon}$, where c is the speed of light and ϵ is the relative permittivity or dielectric constant. The dielectric constant is a property of materials that depends, among other parameters, on their composition, density, and humidity. For dry sedimentary materials, we use the relationship $\epsilon = 1.96 \rho$ [38], where ρ corresponds to the density. By comparing the existing topography with the estimated depth Δh , the relative permittivity of the material can be estimated in regions where there is a topographic elevation above and the reflector is assumed to be in the underlying plane. This can be used to get first-order information about the density of accumulated materials above the reflector, and to extrapolate for other reflectors for which there is no direct topographic comparison. Permittivity values from the Moon can also be used as a reference to provide an estimate of the density, as the lunar layers are typically dry, and have been compared with measurements of samples brought back to Earth [39]. According to data derived from the FRENDS workgroup [40], the water content of the shallowest subsurface is apparently low, which allows us to handle this material as dry volcanic rocks.

To end this section, we present graphically (Figure 2) the steps followed in the interpretation of radargrams, using track 3628101 as an example.

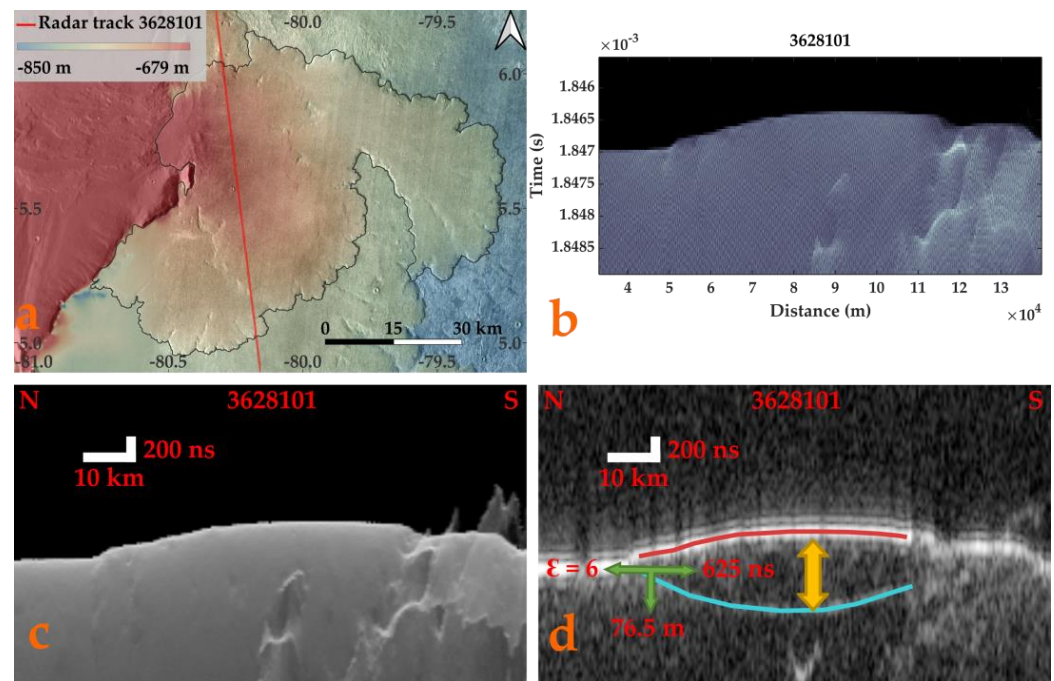


Figure 2. Graphical description of the process used to discriminate true or false subsurface reflectors using SHARAD radargrams, here illustrated with the 3628101 radargram. (a) Track of the radargram over the lava body. (b) Our own cluttergram simulation. (c) PDS simulation cluttergram for this radargram. (d) A radargram with the reflector (blue) that reflects the signal with a travel time of 625 ns. This can be converted to an estimated depth of 76.5 m (assuming $\epsilon = 6$).

3. Results

3.1. Lava Fan and Potential Reflectors

Through visual inspection of THEMIS-derived images and MOLA-derived hillshade, we have found a lava-flow structure located at -80°E , 5.6°N , in the Echus Chasma region that is very well preserved (Figure 3).

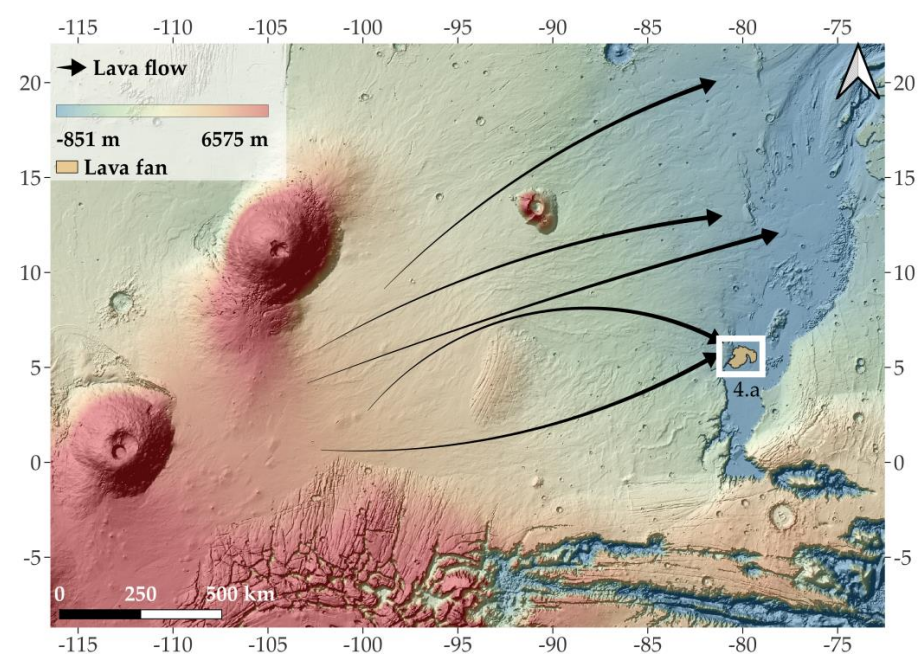


Figure 3. Large-scale lava flow directions from the Asraeus/Pavonis area towards the Echus-Kasei system. MOLA-derived base map.

The direction of the flow is consistent with the orientation of the fan. The elevation of the lava fan is higher than 80 m above the plain of Echus Chasma and its surrounding area (a detail of the topography of this structure across one of SHARAD's tracks is shown in Figure 4). This structure of approximately 3500 km² shows a lobed shape in the margins and is composed of two main bodies: the proximal one has a more massive aspect and is connected by a narrow arm that grows from west to east, and the distal part whose ending consists of a fan-shaped landform with a southerly trend that is consistent with the underlying topography (see Figure 4). This contrasts with the general inclination of the depression, which points to a massive outflow toward the north [41].

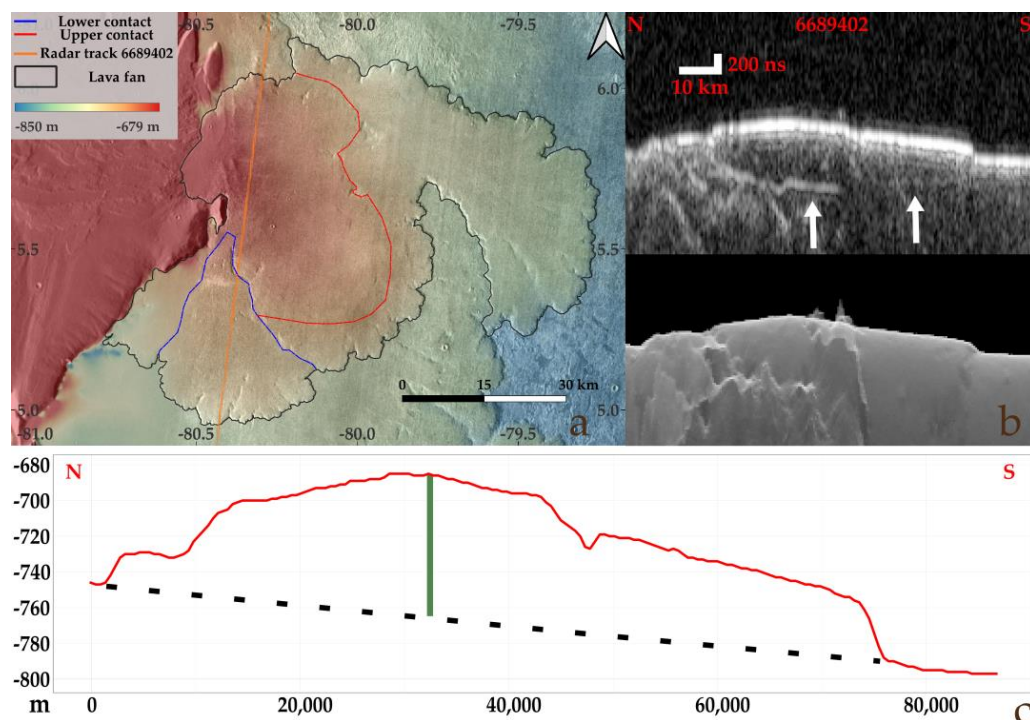


Figure 4. (a) Map showing the structure of the lava flow composed of two distinguishable bodies in radargram 6689402. The orange line marks the radar trajectory. (b) A cross-sectional radargram showing the thickest layer of the fan in its northern part and the thinnest body that forms the southern lobe, and below, the corresponding cluttergram. White arrows indicate the detected reflectors. (c) A topographic profile over MOLA corresponding to the same path. The black dashed line marks the presumed original surface and the green line shows the maximum depth of the main reflector (approximately 80 m).

Analysing surface features, we found vents widely distributed over the entire surface of the lava fan, forming smooth surfaces that mark the direction of flow and are consistent with both the slope and the general direction of growth of the main structure (see Figure 5).

We have analysed 27 SHARAD tracks over this area (Table A1), and we have found potential reflectors in five of them (Figures 6 and A2).

These surfaces present high backscattering, returning high-intensity signals that translate into bright reflectors in the radargrams. The brightness contrast in the radargrams is due to the difference in the dielectric properties of the materials crossed by the radar signal (Figure 7).

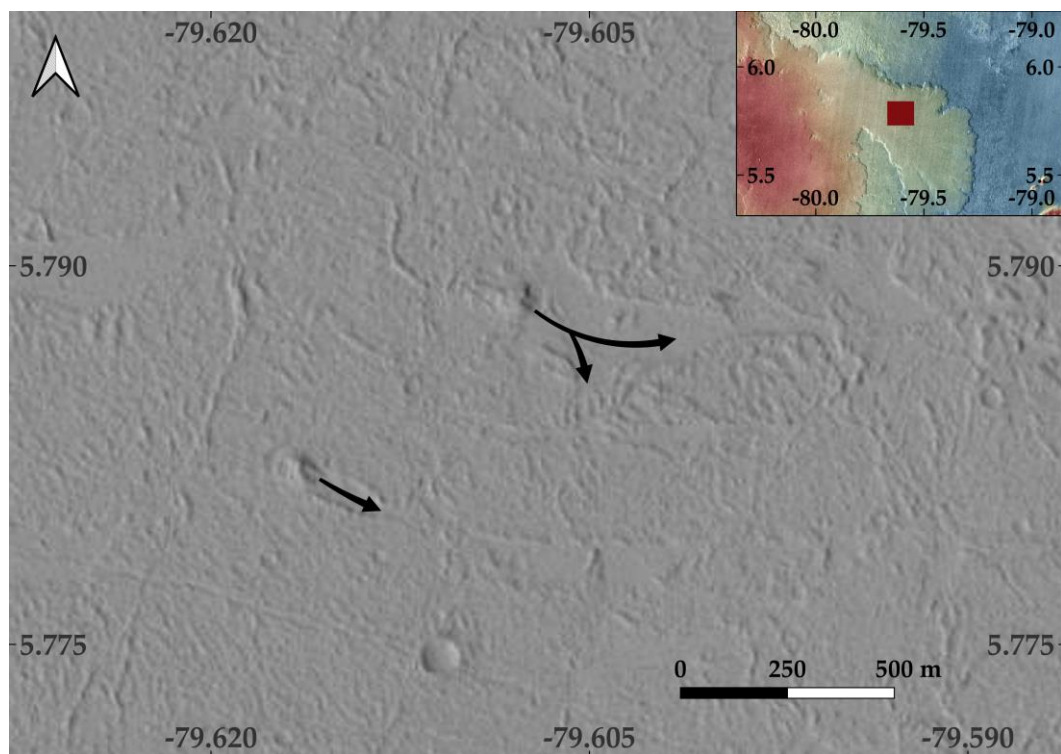


Figure 5. A closer view of the lava vents observed on the surface of the lava fan. Curvilinear black arrows indicate the direction of the flow.

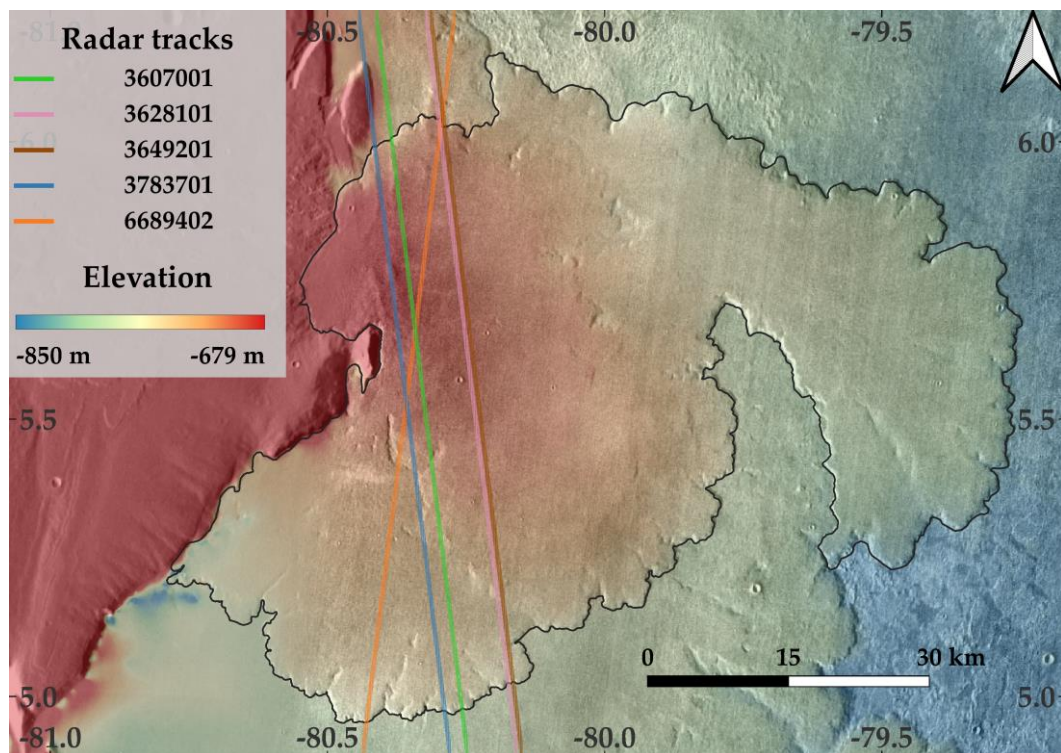


Figure 6. Footprint of the five SHARAD tracks that show preserved reflectors. See Table A1 and Figure A1 for coordinates and traces of the twenty-seven SHARAD tracks analysed in this study.

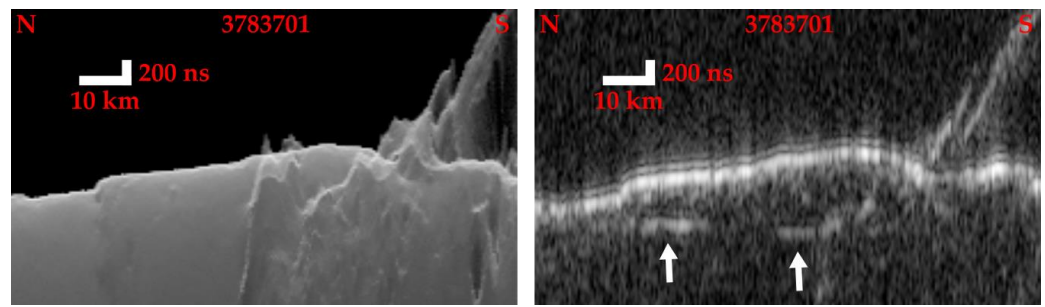


Figure 7. Paired cluttergram vs. radargram for the 3783701, which illustrates a positive case of a true reflector.

3.2. Lava Fan Age

We have next performed a crater counting analysis of the lava fans to date the age of their surface (Figure 8). We have not made any differentiation between the layers of the lava fan because there is not enough confidence in small areas to constrain the age through crater dating. The size of 197 craters found in the lava fan region, which covers an extension of about 3518 km², has been determined. The cumulative crater density for each crater diameter size has been calculated and compared with the age system proposed by Michael (2013) [35]. The lava flow fans are estimated to be only 59 ± 4 Ma old, confirming that this feature is very young. Since all 197 craters seem to follow the same isochrone, we conclude that it is reasonable to interpret that all the lava fans in this structure formed at the same period and have not been modified differently by subsequent processes.

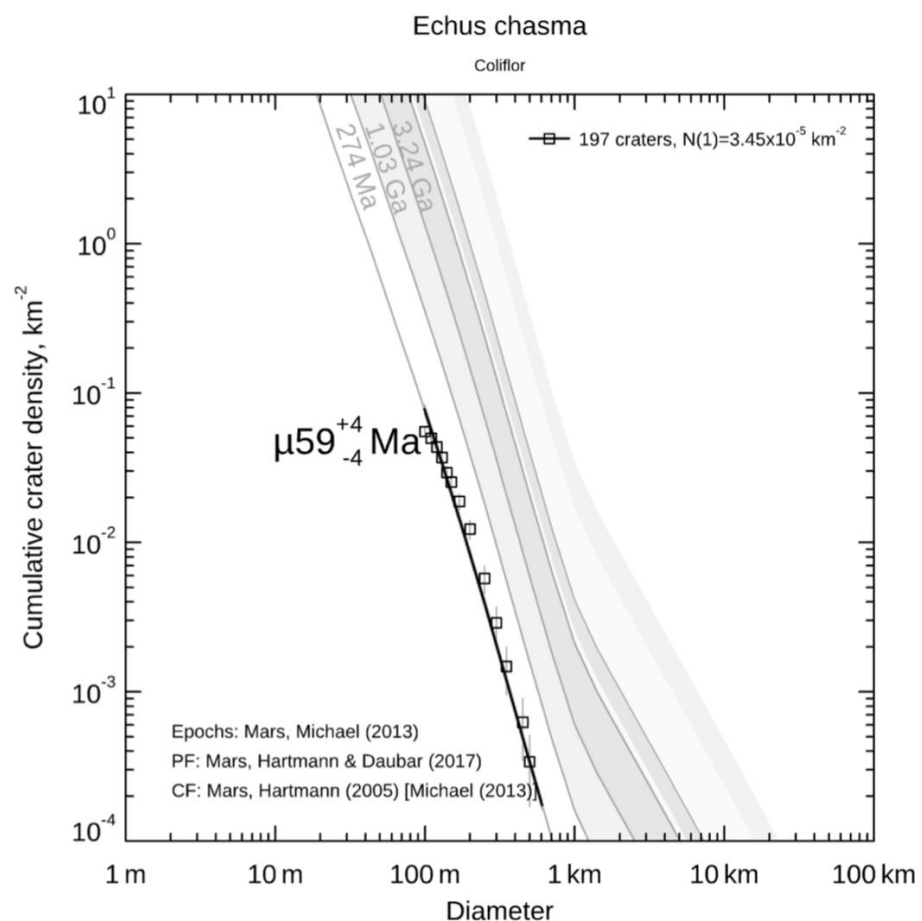


Figure 8. Crater counting dating of the lava fan using Craterstats [35,37,42]. The isochrone suggests an age of 59 ± 4 Ma.

3.3. Depth and Permittivity of Subsurface Layers

We have applied the cluttergram technique to make sure that these reflectors are not artefacts originating from reflections of the surface (Figure 8). Following the method described above, we have found five true reflectors underneath this 59 Ma age structure. For each reflector, we take note of the maximal delay time of the reflector signal. Assuming a dielectric constant, we can retrieve an estimated reflector depth. Figure 2 shows an example of this for $\epsilon = 6$, which is a typical value for sedimentary rocks with a dry density of around 2650 kg/m^3 [38]. To have a range of possible depths to compare with, we can use the lower and upper bounds of possible permittivities, including those estimated for lava flow-like structures on Mars [11]. The resulting ranges of depths for the five reflector layers are summarised in Table 1.

Table 1. Maximum depth of the preserved layers at the Echus Chasma eastern fan [11].

Maximum Depths SWT (Single Wave Travel Time) at Echus Chasma Eastern Fan					
	Longitude (Deg. E)	Latitude (Deg. N)	Δt (ns)	Lower Bound ϵ Estimated Depth (m) $\epsilon = 6.2$ (Carter et al., 2009)	Upper Bound ϵ Estimated Depth (m) $\epsilon = 17.3$ (Carter et al., 2009)
3607001	−80.36	5.79	637.50	77	46
3628101	−80.22	5.43	656.25	79	47
3649201	−80.37	5.61	693.75	84	50
3783701	−80.37	5.63	656.25	79	47
6689402	−80.34	5.71	600.00	72	43

Most of the reflectors are continuous. Some may be apparently intermittent; in those regions, there is less contrast in permittivity. This may be caused by local changes in material properties or orientation (which may affect the radar reflection) or because they might belong to different lava bodies.

The height of the lava fan is of the order of 80 m, so assuming that the subsurface reflectors are at the level of the current base, this suggests that the material has a permittivity close to 6.2, which is in agreement with the values given for Mars by Carter et al., 2009 [11], where they analyse the permittivities of lava flows on the western flank of Ascræus Mons, which we consider equivalent; see Table 1, where we summarize the single wave travel time (SWT) (some authors use TWT—twice wave travel time—but the travel time provided by JMARS refers only to one way $\Delta t = \Delta x \times 37.5/2$, where Δx refers to the incremental in pixels on the radargram).

3.4. Northward Terrains: Subsurface Layers and a Volcanic Pit Chain

A few kilometres towards the north (Figure 9 right), we can also observe a pit chain formed by a collapse along a lava conduit, which was emptied when the volcanic activity stopped (Figure 9 left). These pit caves are well preserved, suggesting that they were formed recently over a relatively fresh structure of lava tubes associated with lava flows from Ascræus Mons.

The radar track analysis shown in Figure 9 right, just a few kilometres to the north of the lava fan, shows a well-preserved, plain-parallel reflector structure. Assuming the same dielectric constant thresholds suggested above, these reflectors can be estimated to be at depths of between 20 and 12 m; see Figure 10 right. The cluttergram shows no sign of bright layers, confirming that these are true plane-parallel reflectors. The footprint of this track lies within the unit At5, described by Chapman et al., 2010 [4], which according to these authors is characterised by young lava flows dated from 89 Ma on average.

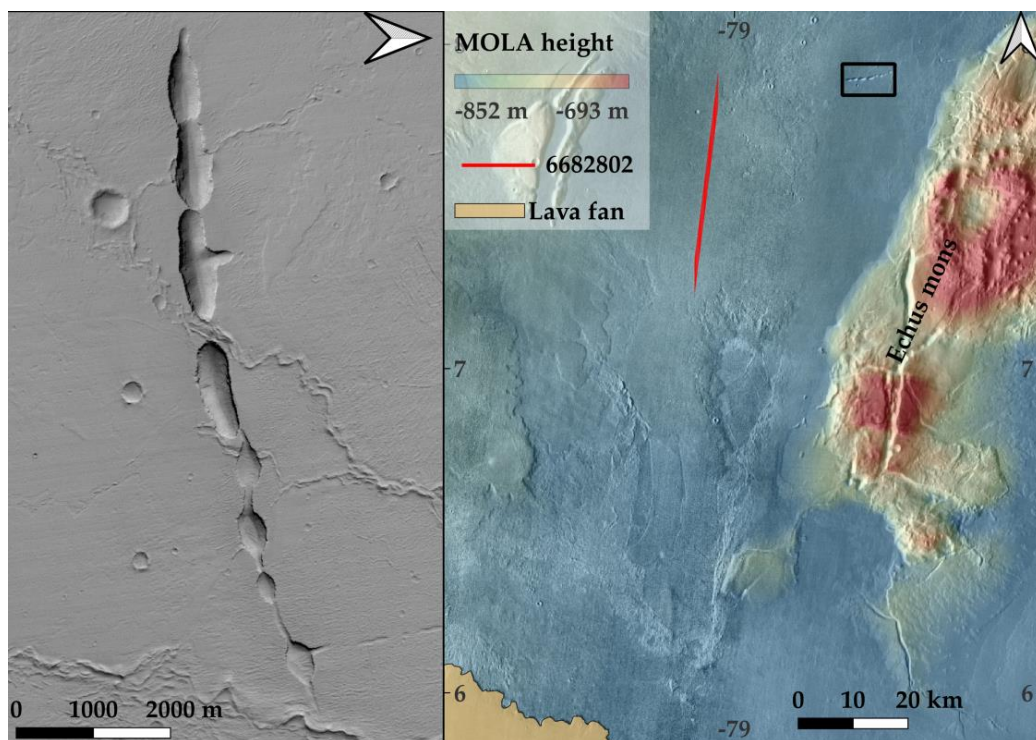


Figure 9. (Left) Image of pit chain observed with CTX at 7.88°N , -8.62°E . (Right) Regional context map (derived from the MOLA base map).

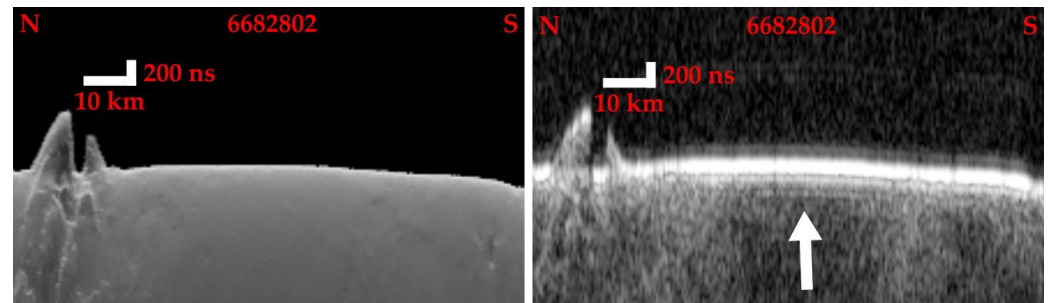


Figure 10. (Left) Cluttergram, where the shallower reflectors do not appear. (Right) Radargram of a north-to-south SHARAD track, 6682802, marked in red in Figure 9, which shows bright subsurface plane parallel reflectors that are not seen in the cluttergram.

4. Discussion

Subsurface reflectors are expected to be preserved only underneath surfaces that have recently occurred. Pristine volcanic surfaces trapped beneath recent deposits could preserve the original fracture system [43] and original porosity. Both tend to collapse over time due to lithostatic pressure and mineral alteration processes.

The importance of the existence of these reflectors is twofold: (1) on one side, their presence is interesting to confirm the relative youth of this unit because, as Stillman and Grim, 2011 [43] describe, these features are only preserved in the youngest geological units; and (2) the contrast in permittivity between the reflector and the material above could indicate variations in the porosity [13], and that may point to the past or present presence of fluids, water ice, volatiles, etc., which may be a potential habitable environment for life.

We have analysed 27 radar tracks of the SHAlow RADAR (SHARAD) instrument on board the Mars Reconnaissance Orbiter (MRO) over the region of Echus Chasma. We have found, underneath a fresh lava flow of about 59 ± 4 Ma years, five subsurface reflectors at depths from 35 to 79 m [13]. Some vents are preserved above this lava flow of >80 m

thickness. During this period, Arsia Mons, the southernmost volcano of Tharsis, was active. Our analysis also demonstrates the volcanic activity of Ascraeus Mons, the northernmost volcano, towards the Echus Chasma region.

The existence of preserved, small-scale, surficial vents suggests that this structure has not been covered later by other materials, which would have easily broken or eroded it. Therefore, it is reasonable to think that the lava fan has not been resurfaced and has been exposed directly to the atmosphere from the moment of its formation until now. This suggests that the dating of this structure is the true formation date and not the duration of the exposure after resurfacing.

Overlying lava flows may have helped preserve past ice or liquid water reservoirs from sublimation and evaporation while also serving as a shield from radiation. Only two meters of rock are needed to shield from space radiation [15], but with SHARAD data, we cannot resolve shallow reflectors (of the order of meters) as they would be fused with the surface signal.

The preservation of reflectors in this region is rare. The exception to this, is the existence of those five unique reflectors close to the base of the cliff, within the widest part of the lava fans. The current height of the lava fan is of the order of 80 m above the floor, which suggests that the material must have had a low permittivity value, such as $\epsilon = 6.2$, so that the depth of the preserved subsurface reflectors is compatible with the measured topography. This permittivity value is the value of lava flows with low density, and porosities are as high as 35% [13].

Our analysis suggest that these fans were formed by high porosity lava flows, which could have been generated by inherent magma degasification or by volatiles provided by an underlying, water-rich material, at the bottom of Echus Chasma. This degasification process would also be consistent with the formation of vents at the surface of the lava fan to facilitate the release of volatiles from the magma [44].

Finding open lava tubes or pit chains within a planet can be a challenging task, as they are relatively small. To detect a lava tube opened to the sky in the present epoch, it is required that the lava process be recent so that the subsurface structures that were produced by the flow of lava have not been exposed to extensive modification and are well preserved. Additionally, the openings need to be big enough that they have not been covered by dust and can be distinguished from the orbit. Our analysis suggests that using orbital radar to find large scale preserved subsurface reflectors in regions that have been recently formed by lava may increase the chances of finding other well-preserved structures associated with lava flow, such as lava tubes. Indeed, within a few kilometres of these preserved subsurface reflectors, there is a collection of well-preserved plane-parallel reflectors, at an estimated depth of only 12 m (or 20 m at most), together with a pristine open pit chain that extends over several kilometres. Both preserved features are consistent with the hypothesis that this is a relatively young region produced by volcanic activity. It is worth indicating that pits and lava tubes are considered “special regions” on Mars [16] with special planetary protection requirements. Lava tubes are considered of interest for the future of human exploration of Mars, and at the same time they are potentially interesting for the present-day habitability of Mars, as they offer shelter from radiation and thermal contrasts and may have access to subsurface water resources.

5. Conclusions

For the current and future exploration of Mars, it is interesting to map the subsurface regions of Mars where the environment may be adequate for life at the present time, creating one of the so-called special regions, defined as regions within which terrestrial organisms are likely to replicate [16]. An example of special regions associated with volcanic activity that are of particular interest for human exploration are lava tubes, caves, and pit chains [17]. We have shown that, mapping well-preserved subsurface layers underneath lava structures allows us to investigate the geological processes that took place in the past that could have formed an encapsulated environment that also protects water, ice, or life from surface

conditions, that could cause sublimation and, as a result, water loss. We suggest the use of a multi-instrumental and remote sensing approach that combines radar measurements with photointerpretation, geological mapping, and topographic analysis.

Using this approach, we discovered five preserved subsurface layers (Figure A2) at a depth of about 80 m within the Echus Chasma system on Mars, protected beneath a young lava flow of about 59 Ma. Within this same structure, there is a fresh, shallow pit chain that extends over several kilometres and may provide direct access to a special region formed about 59 Ma during the last volcanic activity that affected this region.

We conclude that radar instrumentation is a powerful tool for planetary exploration to detect from orbit potential subsurface regions of interest and plan future surface missions.

Author Contributions: Conceptualisation, F.M. and M.-P.Z.; methodology, F.M., M.-P.Z. and J.R.; validation, F.M., M.-P.Z., J.R. and I.G.; formal analysis, F.M.; investigation, F.M., M.-P.Z., J.R. and I.G.; writing—original draft preparation, F.M., M.-P.Z. and J.R.; writing—review and editing, F.M., M.-P.Z., J.R. and I.G.; supervision, M.-P.Z. and J.R.; project administration, M.-P.Z.; funding acquisition, M.-P.Z. All authors have read and agreed to the published version of the manuscript.

Funding: M.-P.Z. and F.M. were supported by grant PID2019-104205GB-C21 funded by the MCIN/AEI/10.13039/501100011033. The work of F. Mansilla is supported by the grant PRE2020-09170, founded by MCIN/AEI/10.13039/501100011033.

Data Availability Statement: Not applicable.

Acknowledgments: This study was made possible by the JMARS and QGIS teams, who provided free and open-source tools to make planetary research affordable for everyone.

Conflicts of Interest: The authors declare no conflict of interest.

Appendix A

Table A1. Compendium of analysed radargrams.

Product_Id	Orbit_Number	Start_Time	Stop_Time	Min_Lat	Max_Lat	Min_Lon	Max_Lon
S_00410001	4100	11-6-07 23:03	11-6-07 23:10	−2.9203	19.8318	279.0911	281.9278
S_01666601	16666	15-2-10 3:49	15-2-10 3:56	−1.8656	20.3096	279.4862	282.2436
S_01822902	18229	16-6-10 22:00	16-6-10 22:07	−3.3982	19.6182	278.2445	281.1048
S_01836702	18367	27-6-10 16:56	27-6-10 17:03	−2.8902	19.8162	278.958	281.7788
S_01844001	18440	3-7-10 8:35	3-7-10 8:43	−2.9821	19.7163	277.6721	280.4944
S_02658202	26582	28-3-12 19:49	28-3-12 19:58	1.571	31.3288	280.0101	283.8356
S_02679301	26793	14-4-12 6:24	14-4-12 6:34	−1.017	31.3151	279.3546	283.4961
S_02700402	27004	30-4-12 16:58	30-4-12 17:08	−0.9893	31.3583	279.1326	283.2766
S_02742601	27426	2-6-12 14:06	2-6-12 14:15	1.5615	29.6277	279.3886	282.9802
S_02763702	27637	19-6-12 0:38	19-6-12 0:47	1.5327	31.3059	279.5775	283.4053
S_03543701	35437	16-2-14 18:57	16-2-14 19:09	−19.8196	19.7662	278.6106	283.5576
S_03564801	35648	5-3-14 5:37	5-3-14 5:44	−2.9793	19.7798	278.1862	281.0312
S_03607001	36070	7-4-14 2:41	7-4-14 3:02	−19.7852	49.6769	273.3545	282.8225
S_03628101	36281	23-4-14 13:14	23-4-14 13:36	−19.7785	49.6844	273.4422	282.9112
S_03649201	36492	9-5-14 23:48	10-5-14 0:00	−19.799	19.7861	277.974	282.9227
S_03684801	36848	6-6-14 17:38	6-6-14 17:50	−19.8186	19.7668	277.7591	282.7086
S_03699302	36993	18-6-14 0:55	18-6-14 1:02	−3.016	19.7426	278.8105	281.6553
S_03762601	37626	6-8-14 8:35	6-8-14 8:47	−19.8187	19.7657	277.7287	282.6791
S_03783701	37837	22-8-14 19:08	22-8-14 19:21	−19.8313	19.7534	277.848	282.7982
S_03797501	37975	2-9-14 14:01	2-9-14 14:12	5.2137	39.3474	280.1568	284.7314
S_03804802	38048	8-9-14 5:40	8-9-14 5:53	−21.7875	19.7817	278.1784	283.3845
S_03922201	39222	8-12-14 16:26	8-12-14 16:46	−14.4381	49.6829	273.8819	282.598
S_06627401	66274	15-9-20 14:14	15-9-20 14:27	−12.8326	29.7481	277.1595	282.6131
S_06682802	66828	28-10-20 17:55	28-10-20 18:04	0.0274	29.7475	279.9733	283.8164
S_06689402	66894	2-11-20 21:17	2-11-20 21:27	0.0246	29.7443	278.9569	282.8028
S_06938802	69388	16-5-21 2:10	16-5-21 2:20	0.036	29.7556	279.9379	283.7863
S_07187401	71874	25-11-21 18:10	25-11-21 18:15	−3.9506	13.7761	278.9445	281.1334

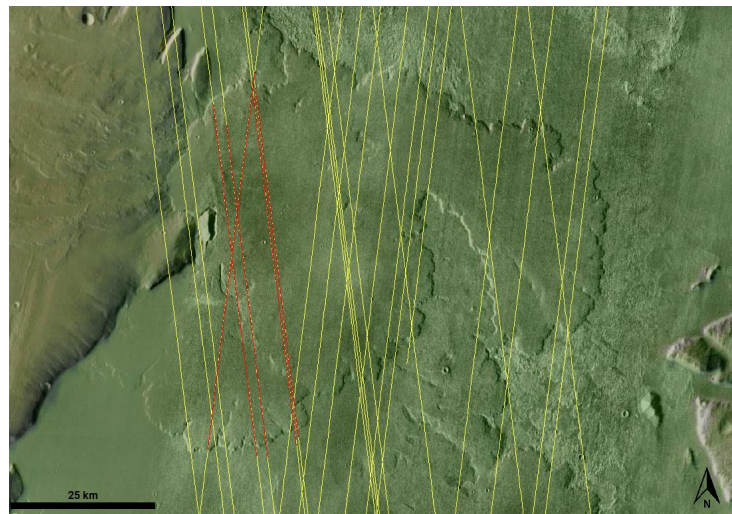


Figure A1. Traces of analysed radargrams are enumerated in Table A1. The marked red traces correspond to the positive cases, marked in bold in Table A1.

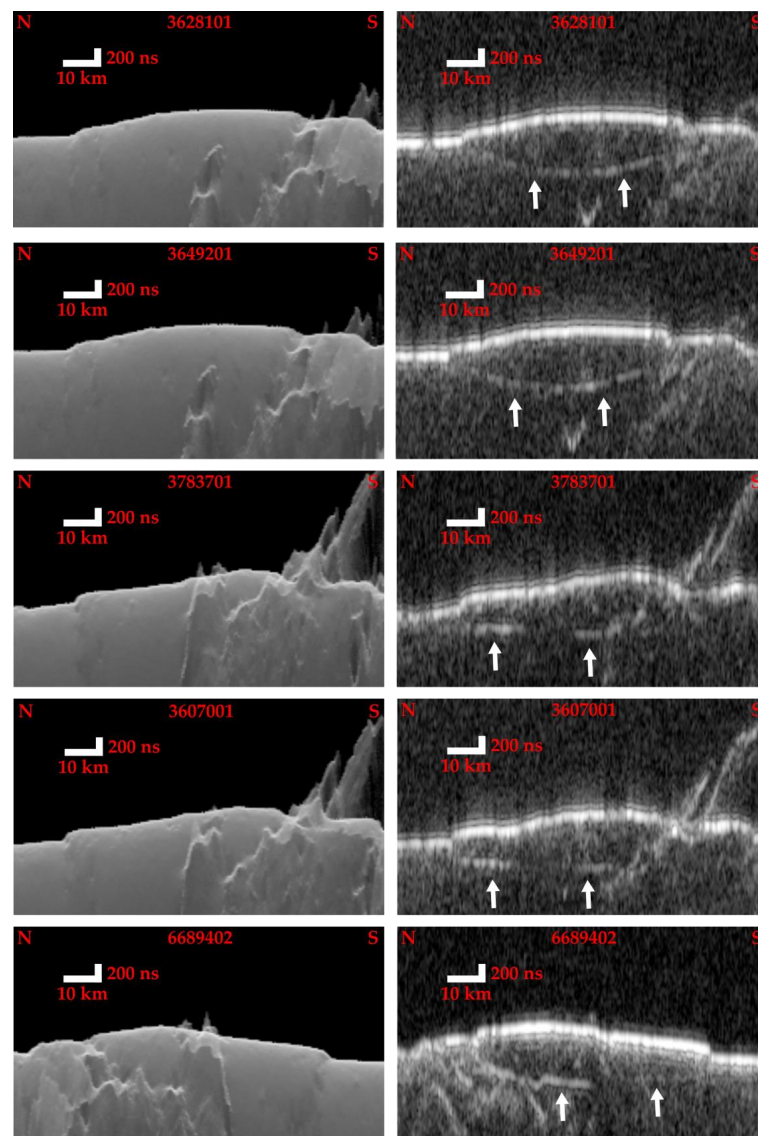


Figure A2. Paired cluttergrams (Left) and radargrams (Right) for each positive case.

References

1. Carr, M.H. The Fluvial History of Mars. *Philos. Trans. R. Soc. Math. Phys. Eng. Sci.* **2012**, *370*, 2193–2215. [CrossRef]
2. Cassanelli, J.P.; Head, J.W. Glaciovolcanism in the Tharsis Volcanic Province of Mars: Implications for Regional Geology and Hydrology. *Planet. Space Sci.* **2019**, *169*, 45–69. [CrossRef]
3. Hepburn, A.J.; Ng, F.S.L.; Holt, T.O.; Hubbard, B. Late Amazonian Ice Survival in Kasei Valles, Mars. *J. Geophys. Res. Planets* **2020**, *125*, e2020JE006531. [CrossRef]
4. Chapman, M.G.; Neukum, G.; Dumke, A.; Michael, G.; van Gasselt, S.; Kneissl, T.; Zuschneid, W.; Hauber, E.; Mangold, N. Amazonian Geologic History of the Echus Chasma and Kasei Valles System on Mars: New Data and Interpretations. *Earth Planet. Sci. Lett.* **2010**, *294*, 238–255. [CrossRef]
5. Chapman, M.G.; Neukum, G.; Dumke, A.; Michael, G.; van Gasselt, S.; Kneissl, T.; Zuschneid, W.; Hauber, E.; Ansan, V.; Mangold, N.; et al. Noachian–Hesperian Geologic History of the Echus Chasma and Kasei Valles System on Mars: New Data and Interpretations. *Earth Planet. Sci. Lett.* **2010**, *294*, 256–271. [CrossRef]
6. Plaut, J.J.; Safaeinili, A.; Holt, J.W.; Phillips, R.J.; Head, J.W.; Seu, R.; Putzig, N.E.; Frigeri, A. Radar Evidence for Ice in Lobate Debris Aprons in the Mid-Northern Latitudes of Mars: RADAR EVIDENCE FOR MID-LATITUDE MARS ICE. *Geophys. Res. Lett.* **2009**, *36*. [CrossRef]
7. Dundas, C.M.; Cushing, G.E.; Keszthelyi, L.P. The Flood Lavas of Kasei Valles, Mars. *Icarus* **2019**, *321*, 346–357. [CrossRef]
8. Richardson, J.A.; Wilson, J.A.; Connor, C.B.; Bleacher, J.E.; Kiyosugi, K. Recurrence Rate and Magma Effusion Rate for the Latest Volcanism on Arsia Mons, Mars. *Earth Planet. Sci. Lett.* **2017**, *458*, 170–178. [CrossRef]
9. Mouginis-Mark, P.J.; Rowland, S.K. Lava Flows at Arsia Mons, Mars: Insights from a Graben Imaged by HiRISE. *Icarus* **2008**, *198*, 27–36. [CrossRef]
10. Hiesinger, H.; Head, J.W.; Neukum, G. Young Lava Flows on the Eastern Flank of Ascraeus Mons: Rheological Properties Derived from High Resolution Stereo Camera (HRSC) Images and Mars Orbiter Laser Altimeter (MOLA) Data. *J. Geophys. Res.* **2007**, *112*, E05011. [CrossRef]
11. Carter, L.M.; Campbell, B.A.; Holt, J.W.; Phillips, R.J.; Putzig, N.E.; Mattei, S.; Seu, R.; Okubo, C.H.; Egan, A.F. Dielectric Properties of Lava Flows West of Ascraeus Mons, Mars. *Geophys. Res. Lett.* **2009**, *36*, L23204. [CrossRef]
12. Shoemaker, E.S.; Carter, L.M.; Garry, W.B.; Morgan, G.A.; Plaut, J.J. New Insights Into Subsurface Stratigraphy Northwest of Ascraeus Mons, Mars, Using the SHARAD and MARSIS Radar Sounders. *J. Geophys. Res. Planets* **2022**, *127*, e2022JE007210. [CrossRef]
13. Rust, A.C.; Russell, J.K.; Knight, R.J. Dielectric Constant as a Predictor of Porosity in Dry Volcanic Rocks. *J. Volcanol. Geotherm. Res.* **1999**, *91*, 79–96. [CrossRef]
14. Cushing, G. Mars Global Cave Candidate Catalog Archive Bundle. *US Geol. Surv. Retrieved Astrogeology Usgs GovsearchmapMars-MarsCaveCatalogmarscavecatalog Zip*. 2017. Available online: <https://doi.org/10.17189/1519222> (accessed on 10 November 2022).
15. Pavlov, A.A.; McLain, H.L.; Glavin, D.P.; Roussel, A.; Dworkin, J.P.; Elsil, J.E.; Yocum, K.M. Rapid Radiolytic Degradation of Amino Acids in the Martian Shallow Subsurface: Implications for the Search for Extinct Life. *Astrobiology* **2022**, *22*, 1099–1115. [CrossRef] [PubMed]
16. Rummel, J.D. Special Regions in Mars Exploration: Problems and Potential. *Acta Astronaut.* **2009**, *64*, 1293–1297. [CrossRef]
17. Sauro, F.; Pozzobon, R.; Massironi, M.; De Berardinis, P.; Santagata, T.; De Waele, J. Lava Tubes on Earth, Moon and Mars: A Review on Their Size and Morphology Revealed by Comparative Planetology. *Earth-Sci. Rev.* **2020**, *209*, 103288. [CrossRef]
18. Lemoine, F.G.; Smith, D.E.; Rowlands, D.D.; Zuber, M.T.; Neumann, G.A.; Chinn, D.S.; Pavlis, D.E. An Improved Solution of the Gravity Field of Mars (GMM-2B) from Mars Global Surveyor. *J. Geophys. Res. Planets* **2001**, *106*, 23359–23376. [CrossRef]
19. Neukum, G.; Jaumann, R. HRSC: The High Resolution Stereo Camera of Mars Express. In *Mars Express: The Scientific Payload*; ESA Publications Division, ESTEC: Noordwijk, The Netherlands, 2004; Volume 1240, pp. 17–35. ISBN 92-9092-556-6.
20. Malin, M.C.; Bell, J.F.; Cantor, B.A.; Caplinger, M.A.; Calvin, W.M.; Clancy, R.T.; Edgett, K.S.; Edwards, L.; Haberle, R.M.; James, P.B.; et al. Context Camera Investigation on Board the Mars Reconnaissance Orbiter. *J. Geophys. Res.* **2007**, *112*, E05S04. [CrossRef]
21. Edwards, C.S.; Nowicki, K.J.; Christensen, P.R.; Hill, J.; Gorelick, N.; Murray, K. Mosaicking of Global Planetary Image Datasets: 1. Techniques and Data Processing for Thermal Emission Imaging System (THEMIS) Multi-Spectral Data. *J. Geophys. Res.* **2011**, *116*, E10008. [CrossRef]
22. QGIS.org, 2022. QGIS Geographic Information System. QGIS Association. Available online: <http://www.qgis.org> (accessed on 10 November 2022).
23. Christensen, P.R.; Engle, E.; Anwar, S.; Dickenshied, S.; Noss, D.; Gorelick, N.; Weiss-Malik, M. JMARS—A Planetary GIS. In Proceedings of the AGU Fall Meeting Abstracts, San Francisco, CA, USA, 14–18 December 2009; Volume 2009, p. IN22A-06.
24. Seu, R.; Biccari, D.; Orosei, R.; Lorenzoni, L.V.; Phillips, R.J.; Marinangeli, L.; Picardi, G.; Masdea, A.; Zampolini, E. SHARAD: The MRO 2005 Shallow Radar. *Planet. Space Sci.* **2004**, *52*, 157–166. [CrossRef]
25. Wilson, A. *Mars Express: The Scientific Payload*; ESA SP; ESA Publications Division: Noordwijk, The Netherlands, 2004; ISBN 978-92-9092-556-9.
26. Holt, J.W.; Peters, M.E.; Kempf, S.D.; Morse, D.L.; Blankenship, D.D. Echo Source Discrimination in Single-Pass Airborne Radar Sounding Data from the Dry Valleys, Antarctica: Implications for Orbital Sounding of Mars. *J. Geophys. Res.* **2006**, *111*, E06S24. [CrossRef]

27. Choudhary, P.; Holt, J.W.; Kempf, S.D. Surface Clutter and Echo Location Analysis for the Interpretation of SHARAD Data From Mars. *IEEE Geosci. Remote Sens. Lett.* **2016**, *13*, 1285–1289. [[CrossRef](#)]
28. Mansilla, F.; Zorzano, M.P.; Giannakis, I.; Ruiz, J. No evidence of reflectors on Jezero radargrams. In Proceedings of the Europlanet Science Congress 2022, Granada, Spain, 18–23 September 2022. EPSC2022-460. [[CrossRef](#)]
29. Putzig, N.E.; Phillips, R.J.; Campbell, B.A.; Plaut, J.J.; Holt, J.W.; Bernardini, F.; Egan, A.F.; Smith, I.B. Custom SHARAD Processing via the CO-SHARPS Processing Boutique. In Proceedings of the 47th Lunar and Planetary Science Conference, Woodlands, TA, USA, 21–25 March 2016; p. 3010.
30. Campbell, B. MRO MARS SHARAD 5 RADARGRAM V2.0. Available online: <https://doi.org/10.17189/YB1W-F075> (accessed on 28 December 2022).
31. Christoffersen, M.S.; Holt, J.W.; Kempf, S.D.; O’Connell, J.D. MRO SHARAD Clutter Simulations Bundle. Available online: <https://doi.org/10.17189/NBDH-2K53> (accessed on 28 December 2022).
32. Hartmann, W.K.; Neukum, G. Cratering Chronology and the Evolution of Mars. *Space Sci. Rev.* **2001**, *96*, 165–194. [[CrossRef](#)]
33. Michael, G.G.; Neukum, G. Planetary Surface Dating from Crater Size–Frequency Distribution Measurements: Partial Resurfacing Events and Statistical Age Uncertainty. *Earth Planet. Sci. Lett.* **2010**, *294*, 223–229. [[CrossRef](#)]
34. Michael, G.G.; Platz, T.; Kneissl, T.; Schmedemann, N. Planetary Surface Dating from Crater Size–Frequency Distribution Measurements: Spatial Randomness and Clustering. *Icarus* **2012**, *218*, 169–177. [[CrossRef](#)]
35. Michael, G.G. Planetary Surface Dating from Crater Size–Frequency Distribution Measurements: Multiple Resurfacing Episodes and Differential Isochron Fitting. *Icarus* **2013**, *226*, 885–890. [[CrossRef](#)]
36. Riedel, C.; Michael, G.; Kneissl, T.; Orgel, C.; Hiesinger, H.; van der Bogert, C.H. A New Tool to Account for Crater Obliteration Effects in Crater Size-Frequency Distribution Measurements. *Earth Space Sci.* **2018**, *5*, 258–267. [[CrossRef](#)]
37. Hartmann, W.K.; Daubar, I.J. Martian Cratering 11. Utilizing Decameter Scale Crater Populations to Study Martian History. *Meteorit. Planet. Sci.* **2017**, *52*, 493–510. [[CrossRef](#)]
38. Carrier, I.W.D.; Olhoeft, G.R.; Mendell, W. Physical Properties of the Lunar Surface. In *Lunar Sourcebook, A User’s Guide to the Moon*; Heiken, G.H., Vaniman, D.T., French, B.M., Eds.; Cambridge University Press: Cambridge, UK; Port Chester, NY, USA, 1991; pp. 475–594. ISBN 978-0-521-33444-0.
39. Heiken, G.; Vaniman, D.; French, B.M. *Lunar Sourcebook: A User’s Guide to the Moon*; Cambridge University Press: Cambridge, UK; Port Chester, NY, USA, 1991; ISBN 978-0-521-33444-0.
40. Malakhov, A.V.; Mitrofanov, I.G.; Golovin, D.V.; Litvak, M.L.; Sanin, A.B.; Djachkova, M.V.; Lukyanov, N.V. High Resolution Map of Water in the Martian Regolith Observed by FRENDE Neutron Telescope Onboard ExoMars TGO. *J. Geophys. Res. Planets* **2022**, *127*, e2022JE007258. [[CrossRef](#)]
41. Williams, R.M.E. Evidence for Late Stage Fluvial Activity in Kasei Valles, Mars. *J. Geophys. Res.* **2004**, *109*, E06001. [[CrossRef](#)]
42. Neukum, G. *Meteoritenbombardement und Datierung Planetarer Oberflächen. Habilitation Dissertation for Faculty Membership*; Ludwig-Maximilians Universität: München, Germany, 1983.
43. Stillman, D.E.; Grimm, R.E. Radar Penetrates Only the Youngest Geological Units on Mars. *J. Geophys. Res.* **2011**, *116*, E03001. [[CrossRef](#)]
44. Edwards, B.; Magnússon, E.; Thordarson, T.; Guðmundsson, M.T.; Höskuldsson, A.; Oddsson, B.; Haklar, J. Interactions between Lava and Snow/Ice during the 2010 Fimmvörðuháls Eruption, South-Central Iceland: 2010 FIMMVÖRÐUHÁLS LAVA-SNOW. *J. Geophys. Res. Solid Earth* **2012**, *117*. [[CrossRef](#)]

Disclaimer/Publisher’s Note: The statements, opinions and data contained in all publications are solely those of the individual author(s) and contributor(s) and not of MDPI and/or the editor(s). MDPI and/or the editor(s) disclaim responsibility for any injury to people or property resulting from any ideas, methods, instructions or products referred to in the content.